# Appendices

# Appendix A

**Abstract** In this appendix, we develop an analytical framework for dealing with mosaic spread and discuss experimental techniques to measure the degree of mosaic spread.

## A.1 Mosaic Spread for NFIT Analysis

First we calculate how mosaic spread affects the structure factor S(q). Next we discuss two experimental methods. Third, we discuss the updated NFIT program. Fourth, we show the results.

### *A.1.1 Mosaic Spread: Calculation*

In this section, an analytical framework for dealing with mosaic spread is developed. A sample of oriented stacks of bilayers consists of many small domains, within which layers are registered in an array. An ideal domain is a domain where the layers are parallel to the substrate, whose surface is in the sample *xy*-plane, so the orientation **n** of an ideal domain is perpendicular to the substrate as shown in Fig. A.1. In general, the orientation $\mathbf{n}'$ of a domain is tilted from that of an ideal domain by some angle $\alpha$. Then, we consider a mosaic spread distribution function, $P(\alpha)$, representing a probability of finding a domain with a tilt $\alpha$. We assume that the sample is symmetric about the substrate normal, so that the distribution $P(\alpha)$ does not depend on the azimuthal angle, $\beta$. The normalization condition on $P(\alpha)$ is

$$1 = \int_0^{2\pi} d\beta \int_0^{\frac{\pi}{2}} d\alpha \sin\alpha P(\alpha). \tag{A.1}$$

The object of this section is to derive the X-ray scattering structure factor including the distribution function $P(\alpha)$.

First, let us consider a two dimensional example. Our sample consists of two identical domains except a tilt $\alpha$ shown in Fig. A.2. Then, the sample structure factor



K. Akabori, *Structure Determination of HIV-1 Tat/Fluid Phase Membranes and DMPC Ripple Phase Using X-Ray Scattering*, Springer Theses,
DOI 10.1007/978-3-319-22210-3

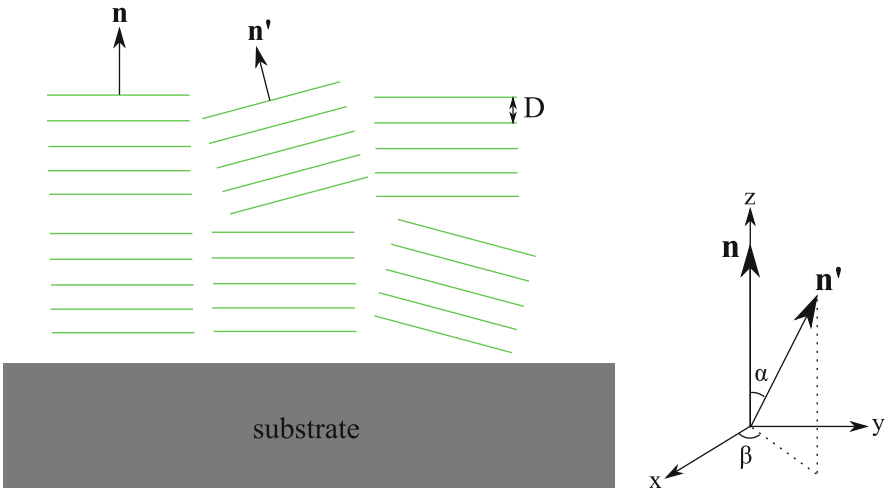


**Fig. A.1** Two dimensional view of mosaic spread (*left*) and notations used in this section (*right*). The stacking direction of an ideal domain is **n** and that of a tilted domain **n**′. The deviation of **n**′ from **n** denoted as $\alpha$ quantifies the degree of misorientation of a domain. The $x$, $y$, and $z$-axes are the sample coordinates

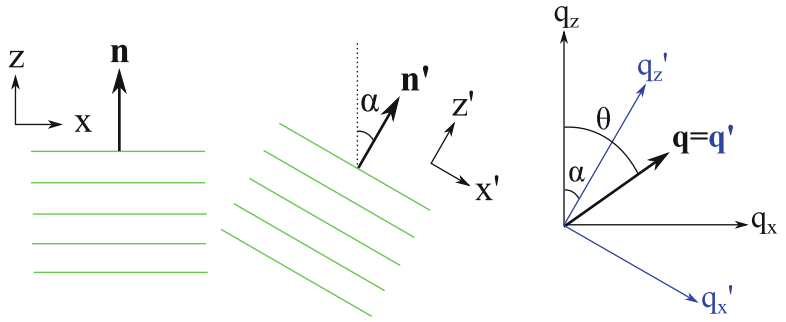


**Fig. A.2** Example of a two dimensional sample consisting of an ideal and tilted domains. $\mathbf{q} = (q_x, q_z)$ is the sample $q$-space and $\mathbf{q}' = (q'_x, q'_z)$ is the domain $q$-space. The two $q$-spaces are related by a rotation of $\alpha$ about the $y$-axis, which is into the page

$S^{\text{sam}}(\mathbf{q})$ is a superposition of the structure factor $S(\mathbf{q})$ of the ideal domain and $S(\mathbf{q}')$ of the tilted domain,

$$S^{\text{sam}}(\mathbf{q}) = S(q_x, q_z) + S(q'_x, q'_z). \tag{A.2}$$

To express $S(q'_x, q'_z)$ in terms of the sample $q$-space $(q_x, q_z)$, we write $q'_x$ and $q'_z$ in terms of $q_x$, $q_z$, and $\alpha$,

$$
\begin{aligned}
q'_x &= \mathbf{q}\cdot\hat{\mathbf{x}}' = q\cos\left(\frac{\pi}{2}-\theta+\alpha\right)\\
q'_z &= \mathbf{q}\cdot\hat{\mathbf{z}}' = q\sin\left(\frac{\pi}{2}-\theta+\alpha\right)\\
q_x &= q\cos(\pi/2-\theta)\\
q_z &= q\sin(\pi/2-\theta)
\end{aligned}
\tag{A.3}
$$

where $q = |\mathbf{q}|$. Equations (A.2) and (A.3) give the structure factor of a sample consisting of the two domains. With a continuous distribution of $\mathbf{n}'$, we integrate over the angle $\alpha$ with each structure factor modulated by the distribution function $P(\alpha)$,

$$
S_M(\mathbf{q}) = S_M(q,\theta) = \int_{-\frac{\pi}{2}}^{\frac{\pi}{2}} d\alpha\, S(q'_x, q'_z)P(\alpha), \tag{A.4}
$$

Variables $q$ and $\theta$ are used in the above equation to make a connection with the three dimensional case, where the spherical coordinates are convenient, which we discuss now.

For a three dimensional sample, the basic idea is the same as the two dimensional case. In the three dimensional case, we also rotate the vector $\mathbf{n}'$ about the $z$-axis by an angle $\beta$ after the rotation about the $y$-axis by an angle $\alpha$, so all we need to do is to apply appropriate rotation matrices to the sample $xyz$-axes which define the domain coordinates $x'y'z'$.

The rotation matrix for rotating a vector about the $y$-axis is given by

$$
R_y = \begin{pmatrix} \cos\alpha & 0 & \sin\alpha \\ 0 & 1 & 0 \\ -\sin\alpha & 0 & \cos\alpha \end{pmatrix} \tag{A.5}
$$

and for rotating about the $z$-axis

$$
R_z = \begin{pmatrix} \cos\beta & -\sin\beta & 0 \\ \sin\beta & \cos\beta & 0 \\ 0 & 0 & 1 \end{pmatrix}. \tag{A.6}
$$

Then, what we want is

$$
\hat{\mathbf{x}}' = R_z R_y \begin{pmatrix} 1 \\ 0 \\ 0 \end{pmatrix} = \begin{pmatrix} \cos\alpha\cos\beta \\ \cos\alpha\sin\beta \\ -\sin\alpha \end{pmatrix} \tag{A.7}
$$

$$
\hat{\mathbf{y}}' = R_z R_y \begin{pmatrix} 0 \\ 1 \\ 0 \end{pmatrix} = \begin{pmatrix} -\sin\beta \\ \cos\beta \\ 0 \end{pmatrix} \tag{A.8}
$$

$$\hat{\mathbf{z}}' = R_z R_y \begin{pmatrix} 0 \\ 0 \\ 1 \end{pmatrix} = \begin{pmatrix} \sin\alpha\cos\beta \\ \sin\alpha\sin\beta \\ \cos\alpha \end{pmatrix}. \tag{A.9}$$

The domain $q$-space, $(q'_x, q'_y, q'_z)$, in terms of the sample $q$-space $(q_x, q_y, q_z)$ is given by

$$q'_x = \mathbf{q}\cdot\hat{\mathbf{x}}' = q_x\cos\alpha\cos\beta + q_y\cos\alpha\sin\beta - q_z\sin\alpha, \tag{A.10}$$

$$q'_y = \mathbf{q}\cdot\hat{\mathbf{y}}' = -q_x\sin\beta + q_y\cos\beta, \tag{A.11}$$

$$q'_z = \mathbf{q}\cdot\hat{\mathbf{z}}' = q_x\sin\alpha\cos\beta + q_y\sin\alpha\sin\beta + q_z\cos\alpha. \tag{A.12}$$

The transformation expressed in the spherical coordinates is

$$\cos\theta' = \frac{q'_z}{q} = \sin\theta\sin\alpha\cos(\phi-\beta) + \cos\theta\cos\alpha, \tag{A.13}$$

$$\tan\phi' = \frac{q'_y}{q'_x} = \frac{\sin\theta\sin(\phi-\beta)}{\sin\theta\cos\alpha\cos(\phi-\beta) - \cos\theta\sin\alpha}. \tag{A.14}$$

Summing over all the domains, we get for the mosaic spread modified structure factor

$$S_M(q,\theta,\phi) = \int_0^{2\pi} d\beta \int_0^{\frac{\pi}{2}} d\alpha\, S(q,\theta',\phi')P(\alpha) \tag{A.15}$$

with Eqs. (A.13) and (A.14).

To test these equations, let us apply them to the simple case of a stack of rigid layers with their normals parallel to the $z$-axis in spherical coordinates. The structure factor is then

$$S(q,\theta,\phi) = \frac{\delta(q-\frac{2\pi h}{D})}{q^2}\delta(\cos\theta - 1)\delta(\phi) \tag{A.16}$$

where $\delta(x)$ is the Dirac delta function. From Eq. (A.14), $\delta(\phi')$ is equivalent to $\delta(\beta-\phi)$. Setting $\beta = \phi$ in Eq. (A.13) gives $\cos\theta' = \cos(\alpha-\theta)$. Then, the mosaic spread modified structure factor $S_M(\mathbf{q})$ is

$$\begin{aligned} S_M(q,\theta,\phi) &= \int d\alpha \int d\beta\, \frac{\delta(q-\frac{2\pi h}{D})}{q^2}\delta(\cos\theta' - 1)\delta(\beta-\phi)P(\alpha) \\ &= \frac{\delta(q-\frac{2\pi h}{D})}{q^2}\int d\alpha\, \delta(\cos[\alpha-\theta]-1)P(\alpha) \\ &= \frac{\delta(q-\frac{2\pi h}{D})}{q^2}P(\theta). \end{aligned} \tag{A.17}$$

Equation (A.17) describes hemispherical shells with radii of $2\pi h/D$ in the sample $q$-space. As will be described in the next section, a 2D detector records cross sections of these shells, which give rise to mosaic arcs along $q = 2\pi h/D$.

The structure factor of thermally fluctuating layers is not simple delta functions and gives rise to diffuse scattering. Analysis of the diffuse scattering from a sample with mosaic spread requires Eq. (A.15).

### *A.1.2 Mosaic Spread: Near Equivalence of Two Methods*

In this section, we discuss experimental procedures to probe appropriate $q$-space to measure the mosaic spread distribution, $P(\alpha)$. In our setup, the angle of incidence between the beam and substrate, denoted by $\omega$, can be varied. A conventional method to measure $P(\alpha)$ is a rocking scan, where one measures the integrated intensity of a given Bragg peak as a function of $\omega$ with a fixed detector position. Another method that takes an advantage of an area detector [1] measures the intensity as a function of $\chi$ on a two dimensional detector (see Fig. A.3). This method has been used to quantify complete pole figures for thin films with fiber texture (isotropic in-plane orientation) [2]. First, we want to compare the two methods mentioned above and determine their relationship.

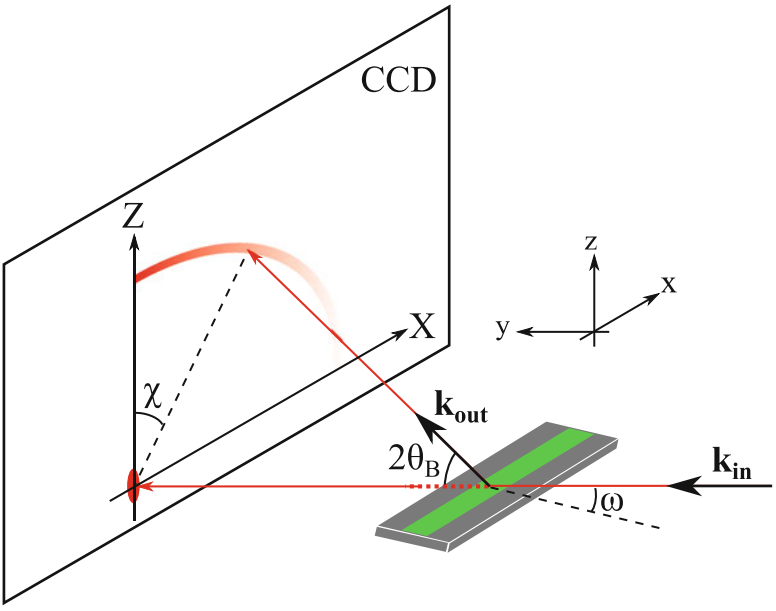


**Fig. A.3** Notations used in this section. The arc originating from the $Z$-axis is the mosaic arc due to the mosaic spread distribution

Equation (3.6) expressed in terms of the coordinates defined in Fig. A.3 is

$$\begin{aligned} q_x &= q\cos\theta\sin\chi \\ q_y &= q\left(-\sin\theta\cos\omega + \cos\theta\cos\chi\sin\omega\right) \\ q_z &= q\left(\sin\theta\sin\omega + \cos\theta\cos\chi\cos\omega\right). \end{aligned} \tag{A.18}$$

For a rocking scan focused on a particular order, $\chi = 0$ and $\theta = \theta_B$ while $\omega$ is varied about $\theta_B$, where $\theta_B$ is the Bragg angle. Then,

$$\begin{aligned} q_x &= 0 \\ q_y &= q_B\sin(\omega - \theta_B) \\ q_z &= q_B\cos(\omega - \theta_B), \end{aligned} \tag{A.19}$$

which shows that this scan traces a part of the circular path in the $q_x = 0$ plane as shown in Fig. A.4. As Fig. A.4 shows, however, the rocking scan only probes a small fraction of the entire distribution, limited by $2\theta_B$. As discussed in Sect. 3.3.2, beyond $\omega = 2\theta_B$, the substrate blocks scattering. On the other hand, the ring analysis takes advantage of a two dimensional detector and can probe a substantially wider range of the distribution in principle: approximately $\pm 45°$ at $\omega = \theta_B$. This method is now described.

In the ring method, we set $\omega = \theta_B$ and scan on the detector along $\theta = \theta_B$ as a function of $\chi$. Then, Eq. (A.18) becomes

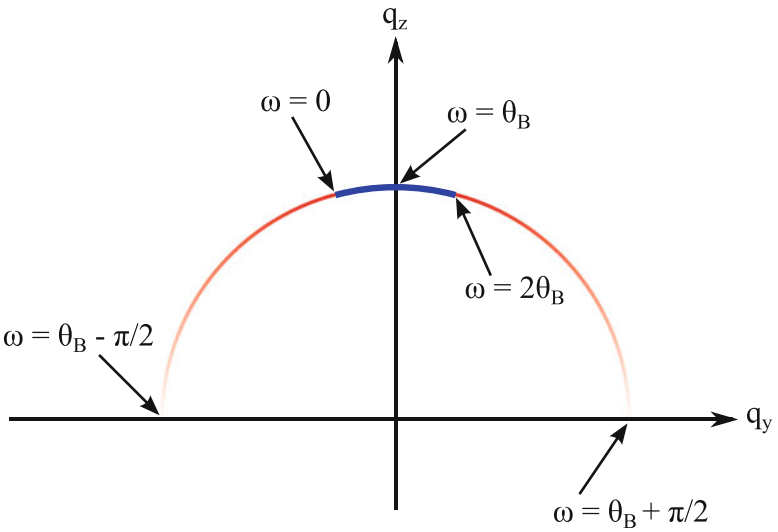


**Fig. A.4** Rocking scan trace in $q$-space

$$
\begin{aligned}
q_x &= q \cos\theta_B \sin\chi \\
q_y &= q \sin\theta_B \cos\theta_B (\cos\chi - 1) \\
q_z &= q(\sin^2\theta_B + \cos^2\theta_B \cos\chi),
\end{aligned} \tag{A.20}
$$

where $q = 4\pi \sin\theta_B/\lambda$. For small $\theta_B$, Eq. (A.20) reduces to

$$
\begin{aligned}
q_x &\approx q \sin\chi \\
q_y &\approx 0 \\
q_z &\approx q \cos\chi.
\end{aligned} \tag{A.21}
$$

For a sharp Bragg peak, this ring method gives the same mosaic intensity $I(\chi, \theta_B)$ in Eq. (A.21) as the rocking method mosaic intensity $I(\omega - \theta_B)$ in Eq. (A.19) because the mosaic distribution $P(\alpha)$ is in-plane isotropic. Differences occur when diffuse scattering is added. The diffuse scattering intensity is much broader and weaker than the Bragg peaks. In the ring method, it can be estimated as the average from two rings offset on either side from $\theta_B$ and subtracted from the $\theta_B$ ring.

### *A.1.3 NFIT*

The original NFIT program was written by Dr. Yufeng Liu and described in his thesis. It was used in the Nagle lab, with small updates for data handling, from 2003 until recently. A newer version has been implemented by Michael Jablin that calculates the theoretical structure factor using cylindrical domains appropriate for in-plane correlations [3] rather than rectangular domains appropriate for coherence domains. All these versions approximated the effect of mosaic spread roughly by averaging only in the $q_r$ direction at fixed $q_z$ which means that mosaic rings are approximated as mosaic lines or spikes. The subsequent development described here and not yet adopted by the Nagle lab calculates the structure factor $S(q_r, q_z)$ with rotational symmetry about the $z$-axis, which eliminates the $\phi'$ dependence in Eq. (A.15). The program interpolates $S(q_r, q_z)$ in terms of the spherical coordinates $q$ and $\theta$ with $\phi = 0$ to perform the double integration in Eq. (A.15). After the mosaic spread integration, the program performs the $q_y$ integration described in Sect. 2.2.5. For this integration, the calculated $S_M$ is interpolated in terms of $q_x$, $q_y$, and $q_z$.

Note: if the structure factor defined in the Cartesian coordinates is desired (for a case of square domains instead of circular ones), Eqs. (A.10), (A.11), and (A.12) can be used instead of Eqs. (A.13) and (A.14).

While it is an improvement, the new program also is an approximation because it does not include the unknown form factor $|F(q_z)|$. The mosaic spread integration mixes up intensity at different $q_z$ values, so the separation of $|F(q_z)|$ from $S(\mathbf{q})$ is in principle impossible. One way to deal with this issue would be to combine the

SDP program, which determines $|F(q_z)|$, with the NFIT program, but that will end up with too many non-linear parameters. Another possibility is to limit the fitting range to regions close to the meridian. For a small range of integration, it is not unreasonable to assume that the form factor is approximately constant as can be seen from Eq. (A.12) with small $q_x$, $q_y$, and $\alpha$. Therefore, the analysis developed in this appendix ignores the form factor.

## A.2 Derivation of the Contour Part of the Form Factor

In this section, we derive $F_{\mathrm{C}}$. The ripple profile, $u(x)$ is given by

$$u(x) = \begin{cases} -\frac{A}{\lambda_r - x_0}\left(x + \frac{\lambda_r}{2}\right) & \text{for } -\frac{\lambda_r}{2} \le x < -\frac{x_0}{2} \\ \frac{A}{x_0}x & \text{for } -\frac{x_0}{2} \le x \le \frac{x_0}{2} \\ -\frac{A}{\lambda_r - x_0}\left(x - \frac{\lambda_r}{2}\right) & \text{for } \frac{x_0}{2} < x \le \frac{\lambda_r}{2} \end{cases} \tag{A.22}$$

The contour part of the form factor is the Fourier transform of the contour function, $C(x, z)$,

$$F_{\mathrm{C}}(\mathbf{q}) = \frac{1}{\lambda_r}\int_{-\frac{\lambda_r}{2}}^{\frac{\lambda_r}{2}} dx \int_{-\frac{D}{2}}^{\frac{D}{2}} dz\, C(x,z) e^{iq_z z} e^{iq_x x}$$

As discussed in section X, the modulated models allow the electron density to modulate along the ripple direction, $x$. This means

$$\begin{aligned} C(x,z) = &\begin{cases} f_1\delta[z - u(x)] & \text{for } -\frac{\lambda_r}{2} \le x < -\frac{x_0}{2} \\ \delta[z - u(x)] & \text{for } -\frac{x_0}{2} < x < \frac{x_0}{2} \\ f_1\delta[z - u(x)] & \text{for } \frac{x_0}{2} \le x < \frac{\lambda_r}{2} \end{cases} \\ &+ f_2\,\delta\left(x + \frac{x_0}{2}\right)\delta\left(z + \frac{A}{2}\right) + f_2\,\delta\left(x - \frac{x_0}{2}\right)\delta\left(z - \frac{A}{2}\right). \end{aligned} \tag{A.23}$$

The contribution from the minor arm is

$$\begin{aligned} &\frac{1}{\lambda_r}\int_{-\frac{\lambda_r}{2}}^{-\frac{x_0}{2}} dx\, e^{iq_x x} e^{iq_z u(x)} + \int_{\frac{x_0}{2}}^{\frac{\lambda_r}{2}} dx\, e^{iq_x x} e^{iq_z u(x)} \\ &= \frac{1}{\lambda_r}\int_{\frac{x_0}{2}}^{\frac{\lambda_r}{2}} dx\, e^{-i\left[q_x x - q_z \frac{A}{\lambda_r - x_0}\left(x - \frac{\lambda_r}{2}\right)\right]} + \int_{\frac{x_0}{2}}^{\frac{\lambda_r}{2}} dx\, e^{i\left[q_x x - q_z \frac{A}{\lambda_r - x_0}\left(x - \frac{\lambda_r}{2}\right)\right]} \\ &= \frac{2}{\lambda_r}\int_{\frac{x_0}{2}}^{\frac{\lambda_r}{2}} \cos\left[\left(q_x - q_z\frac{A}{\lambda_r - x_0}\right)x + q_z\frac{A}{\lambda_r - x_0}\frac{\lambda_r}{2}\right] \end{aligned} \tag{A.24}$$

Using a trigonometric identity,

$$\sin u - \sin v = 2\cos[(u+v)/2]\sin[(u-v)/2],$$

and defining

$$\omega(\mathbf{q}) = \frac{1}{2}\left(q_x x_0 + q_z A\right), \tag{A.25}$$

we further simplify Eq. (A.24),

$$\begin{aligned}
&= \frac{2}{\lambda_r}\frac{\lambda_r - x_0}{\frac{1}{2}q_x\lambda_r - \omega}\cos\left[\frac{1}{2}\left(\frac{1}{2}q_x\lambda_r + \omega\right)\right]\sin\left[\frac{1}{2}\left(\frac{1}{2}q_x\lambda_r - \omega\right)\right] \\
&= \frac{1}{\lambda_r}\frac{\lambda_r - x_0}{\frac{1}{2}q_x\lambda_r - \omega}\cos\left[\frac{1}{2}\left(\frac{1}{2}q_x\lambda_r + \omega\right)\right]\frac{\sin\left(\frac{1}{2}q_x\lambda_r - \omega\right)}{\cos\left[\frac{1}{2}\left(\frac{1}{2}q_x\lambda_r - \omega\right)\right]} \\
&= \frac{\lambda_r - x_0}{\lambda_r}\frac{\cos\left[\frac{1}{2}\left(\frac{1}{2}q_x\lambda_r + \omega\right)\right]}{\cos\left[\frac{1}{2}\left(\frac{1}{2}q_x\lambda_r - \omega\right)\right]}\frac{\sin\left(\frac{1}{2}q_x\lambda_r - \omega\right)}{\frac{1}{2}q_x\lambda_r - \omega}.
\end{aligned} \tag{A.26}$$

Similarly, we calculate the contribution from the major arm,

$$\begin{aligned}
\frac{1}{\lambda_r}\int_{-\frac{x_0}{2}}^{\frac{x_0}{2}} dx\, e^{i\left(\frac{q_z A}{x_0} + q_x\right)x} &= \frac{2}{\lambda_r}\int_0^{\frac{x_0}{2}} dx\cos\left(\frac{q_z A}{x_0} + q_x\right)x \\
&= \frac{x_0}{\lambda_r}\frac{\sin\omega}{\omega}
\end{aligned} \tag{A.27}$$

The contribution from the kink region is

$$\begin{aligned}
&\frac{1}{\lambda_r}\iint dx\,dz\left[\delta\left(x + \frac{x_0}{2}\right)\delta\left(z + \frac{A}{2}\right) + \delta\left(x - \frac{x_0}{2}\right)\delta\left(z - \frac{A}{2}\right)\right]e^{iq_x x}e^{iq_z z} \\
&\quad = \frac{2}{\lambda_r}\cos\omega.
\end{aligned} \tag{A.28}$$

Therefore,

$$\begin{aligned}
F_{\mathrm{C}}(\mathbf{q}) = \frac{x_0}{\lambda_r}\frac{\sin\omega}{\omega} &+ f_1\frac{\lambda_r - x_0}{\lambda_r}\frac{\cos\left[\frac{1}{2}\left(\frac{1}{2}q_x\lambda_r + \omega\right)\right]}{\cos\left[\frac{1}{2}\left(\frac{1}{2}q_x\lambda_r - \omega\right)\right]}\frac{\sin\left(\frac{1}{2}q_x\lambda_r - \omega\right)}{\frac{1}{2}q_x\lambda_r - \omega} \\
&+ \frac{2f_2}{\lambda_r}\cos\omega
\end{aligned} \tag{A.29}$$

To allow different transbilayer models for the major and minor arms, we can write the form factor as

$$F(\mathbf{q}) = F_C^M(\mathbf{q})F_T^M(\mathbf{q}) + f_1F_C^m(\mathbf{q})F_T^m(\mathbf{q}) + f_2F_C^k(\mathbf{q})F_T^k(\mathbf{q}) \tag{A.30}$$

such that

$$F_C^M = \frac{x_0}{\lambda_r}\frac{\sin\omega}{\omega} \tag{A.31}$$

$$F_C^m = \frac{\lambda_r - x_0}{\lambda_r}\frac{\cos\left[\frac{1}{2}\left(\frac{1}{2}q_x\lambda_r + \omega\right)\right]}{\cos\left[\frac{1}{2}\left(\frac{1}{2}q_x\lambda_r - \omega\right)\right]}\frac{\sin\left(\frac{1}{2}q_x\lambda_r - \omega\right)}{\frac{1}{2}q_x\lambda_r - \omega} \tag{A.32}$$

$$F_C^k = \frac{2}{\lambda_r}\cos\omega. \tag{A.33}$$

In this thesis, we employed the same model for $F_T^M$, $F_T^m$, and $F_T^k$, but one could also implement a gel phase model for $F_T^M$ and interdigitated and fluid phase models for $F_T^m$.

## A.3 Derivation of the Transbilayer Part of the Form Factor in the 2G Hybrid Model

In this section, we derive the transbilayer part of the form factor calculated from the 2G hybrid model discussed in Sect. 3.5. Defining $z' = -x\sin\psi + z\cos\psi$, the Fourier transform of a Gaussian function along the line tilted from $z$-axis by $\psi$ is

$$\begin{aligned}
&\iint dz\,dx\,\rho_{\mathrm{H}i}\exp\left\{-\frac{(z'-Z_{\mathrm{H}i})^2}{2\sigma_{\mathrm{H}i}^2}\right\}\delta(x\cos\psi + z\sin\psi)e^{iq_x x}e^{iq_z z}\\
&\quad= \frac{1}{\cos\psi}\int_{-\frac{D}{2}}^{\frac{D}{2}} dz\,\rho_{\mathrm{H}i}\exp\left\{-\frac{(z - Z_{\mathrm{H}i}\cos\psi)^2}{2\sigma_{\mathrm{H}i}^2\cos^2\psi} + i(q_z - q_x\tan\psi)z\right\}\\
&\quad\approx \rho_{\mathrm{H}i}\sqrt{2\pi}\sigma_{\mathrm{H}i}\exp\left\{i\alpha Z_{\mathrm{H}i} - \frac{1}{2}\alpha^2\sigma_{\mathrm{H}i}^2\right\}
\end{aligned} \tag{A.34}$$

with $\alpha = q_z\cos\psi - q_x\sin\psi$. Using Eq. (A.34) and adding the other side of the bilayer and the terminal methyl term, we get

$$\begin{aligned}
F_{\mathrm{G}} = \sqrt{2\pi}\Bigg[&-\rho_{\mathrm{M}}\sigma_{\mathrm{M}}\exp\left\{-\frac{1}{2}\alpha^2\sigma_{\mathrm{M}}^2\right\}\\
&+\sum_{i=1}^{1\text{ or }2} 2\rho_{\mathrm{H}i}\sigma_{\mathrm{H}i}\cos(\alpha Z_{\mathrm{H}i})\exp\left\{-\frac{1}{2}\alpha^2\sigma_{\mathrm{H}i}^2\right\}\Bigg].
\end{aligned} \tag{A.35}$$

The strip part of the model in the minus fluid convention is

$$\rho_{\mathrm{S}}(z) = \begin{cases} -\Delta\rho & \text{for} \quad 0 \le z < Z_{\mathrm{CH_2}}\cos\psi, \\ 0 & \text{for} \quad Z_{\mathrm{W}}\cos\psi \le z \le D/2, \end{cases} \tag{A.36}$$

where $\Delta\rho = \rho_W - \rho_{CH_2}$. Then, the corresponding Fourier transform is

$$\begin{aligned} F_S &= \iint dz\,dx\, e^{iq_x x} e^{iq_z z} \rho_S(z)\delta(x\cos\psi + z\sin\psi) \\ &= \frac{2}{\cos\psi}\int_0^{Z_{CH_2}\cos\psi} dz\cos\left(\frac{\alpha}{\cos\psi}z\right)(-\Delta\rho) \\ &= -2\Delta\rho\frac{\sin(\alpha Z_{CH_2})}{\alpha}. \end{aligned} \tag{A.37}$$

The bridging part of the model in the minus fluid convention is

$$\rho_B(x,z) = \frac{\Delta\rho}{2}\cos\left[\frac{-\pi}{\Delta Z_H}(z' - Z_W)\right] - \frac{\Delta\rho}{2} \tag{A.38}$$

for $Z_{CH_2}\cos\psi < z < Z_W\cos\psi$, and 0 otherwise. Here, $\Delta Z_H = Z_W - Z_{CH_2}$. Then, for the strip part of the form factor, we have

$$\begin{aligned} F_B &= \iint dz\,dx\, e^{iq_x x} e^{iq_z z}\delta(x\cos\psi + z\sin\psi)\rho_B(x,z) \\ &= \frac{\Delta\rho}{\cos\psi}\int_{Z_{CH_2}\cos\psi}^{Z_W\cos\psi} dz\cos\left(\alpha\frac{z}{\cos\psi}\right)\left\{\cos\left[-\frac{\pi}{\Delta Z_H}\left(\frac{z}{\cos\psi} - Z_W\right)\right] - 1\right\} \\ &= \Delta\rho\left\{\frac{\Delta Z_H\sin\left[\frac{\pi(-u+Z_W)}{\Delta Z_H} + \alpha u\right]}{-2\pi + 2\alpha\Delta Z_H} + \frac{\Delta Z_H\sin\left[\frac{\pi(u-Z_W)}{\Delta Z_H} + \alpha u\right]}{2\pi + 2\alpha\Delta Z_H} - \frac{\sin(\alpha u)}{\alpha}\right\}\Bigg|_{Z_{CH_2}}^{Z_W} \\ &= -\frac{\Delta\rho}{\alpha}[\sin(\alpha Z_W) - \sin(\alpha Z_{CH_2})] \\ &\quad + \frac{\Delta\rho}{2}\left(\frac{1}{\alpha + \frac{\pi}{\Delta Z_H}} + \frac{1}{\alpha - \frac{\pi}{\Delta Z_H}}\right)[\sin(\alpha Z_W) + \sin(\alpha Z_{CH_2})]. \end{aligned} \tag{A.39}$$

Because our X-ray scattering intensity was measured in a relative scale, an overall scaling factor was necessary for a non linear least square fitting procedure. This means that $\Delta\rho$ can be absorbed in the scaling factor. Doing so means that the values of $\rho_{Hi}$ and $\rho_M$ resulting from a fitting procedure are relative to $\Delta\rho$.

## A.4 Correction Due to Refractive Index

$q_z$ needs to be corrected for index of refraction [4].

Let $\theta'$ and $\lambda'$ be the true scattering angle and wavelength within the sample. The wavelength by an energy analyzer, $\lambda$, and the scattering angle calculated from a

position on a CCD detector, $\theta$ are apparent. The correction is not necessary in the horizontal direction. The Snell's law gives

$$n\cos\theta = n'\cos\theta' \tag{A.40}$$

$$n\lambda = n'\lambda'. \tag{A.41}$$

For low angle X-ray scattering, the momentum transfer along $z$ direction is

$$q_z = \frac{4\pi\sin\theta'}{\lambda'} \tag{A.42}$$

$$= \frac{4\pi n'}{n\lambda}\sin\theta' \tag{A.43}$$

$$= \frac{4\pi n'}{n\lambda}\sqrt{1-\cos^2\theta'} \tag{A.44}$$

$$= \frac{4\pi n'}{n\lambda}\sqrt{1-\left(\frac{n}{n'}\cos\theta\right)^2}. \tag{A.45}$$

The apparent scattering angle, $\theta$, is directly related to the vertical pixel position, $p_z$, by

$$\theta = \frac{1}{2}\tan^{-1}\left(\frac{p_z}{S}\right), \tag{A.46}$$

where $S$ is the sample-to-detector distance. The typical units of $S$ and $p_z$ are in mm. In our experimental setup, $n = 1$ and $n' = 0.9999978$ for lipids at $\lambda = 1.18$ Å. $S = 359.7$ mm.

## Bibliography

1. A.B. Rodriguez-Navarro, Registering pole figures using an X-ray single-crystal diffractometer equipped with an area detector. J. Appl. Crystallogr. **40**, 631–634 (2007)
2. J.L. Baker, L.H. Jimison, S. Mannsfeld, S. Volkman, S. Yin, V. Subramanian, A. Salleo, A.P. Alivisatos, M.F. Toney, Quantification of thin film crystallographic orientation using X-ray diffraction with an area detector. Langmuir **26**(11), 9146–9151 (2010)
3. Y. Lyatskaya, Y.F. Liu, S. Tristram-Nagle, J. Katsaras, J.F. Nagle, Method for obtaining structure and interactions from oriented lipid bilayers. Phys. Rev. E **63**(1), 0119071–0119079 (2001)
4. Y. Liu, *New method to obtain strcuture of biomembranes using diffuse X-ray scattering: application to fluid phase DOPC lipid bilayers*. PhD thesis, Carnegie Mellon University, 2003